YALE JOURNAL OF BIOLOGY AND MEDICINE 91 (2018), pp.409-430.

ORIGINAL CONTRIBUTION

YALE JOURNAL OF BIOLOGY AND MEDICINE
YJBM
CELEBRATING 90 YEARS 1928–2018

Patterns of Tracheal Compression in the Thorax of the Ground Beetle, *Platynus decentis*

John S. Hochgraf[a,*], James S. Waters[b], and John J. Socha[a]

[a]*Department of Biomedical Engineering and Mechanics, Virginia Tech, Blacksburg, VA;* [b]*Department of Biology, Providence College, Providence, RI*

Insects breathe using a system of tracheal tubes that ramify throughout the body. Rhythmic tracheal compression (RTC†), the periodic collapse and reinflation of parts of the system, has been identified in multiple taxa, but little is known about the precise dynamics of tube deformation cycles. It has been hypothesized that during RTC, compression occurs synchronously throughout the body, but specific kinematic patterns along the length of individual tracheae may vary. Tube collapse or reinflation that proceeds unidirectionally along the length of a tube may function as a pump to transport air, augmenting gas exchange. This study aims to characterize patterns of tracheal compression in one species of carabid beetle, *Platynus decentis*, to test the hypothesis of directional compression. The internal tracheae of living beetles were visualized using synchrotron x-ray phase contrast imaging at the Advanced Photon Source, Argonne National Laboratory. X-ray video results show that tracheal compression is characterized by the formation of discrete, buckled regions in the tube wall, giving the appearance of "dimpling." Dimple formation in the main dorsal tracheal trunks of the prothorax occurred as two semi-circular fronts that spread symmetrically or directionally along the longitudinal tube axis. In the transverse axis, the main ventral trunks collapsed in the lateral direction, whereas the dorsal trunks collapsed dorsoventrally. Along the length of the ventral thoracic tracheal trunks, collapse and reinflation occurred synchronously in the majority of cycles (75 percent), not sequentially. Synchronous longitudinal compression and consistent dimple formation kinematics within an animal suggest that *Platynus decentis* employs a stereotyped mechanism to produce cycles of tracheal collapse and reinflation, but such compression does not function as a unidirectional pump, at least along the length of the local trachea. Further data on spiracle opening and closing patterns and internal pressures within the tracheal system are required to determine actual airflow patterns within the body.

INTRODUCTION

Insects breathe using a tracheal system (Figure 1), delivering oxygen directly to the tissues using a network of tracheal tubes and in some species, air sacs [1]. Atmospheric air enters through valves called spiracles and is transported through the network to tracheoles, the small (~µm diameter), blind-ended tubes where gases diffuse to and from the surrounding cells. Carbon dioxide gases are removed through the system in reverse, from the cells to the spiracles. Within the system, the transport of respiratory gases occurs in two modes [2]. Diffusion is always employed, and in some insects it appears to be the only form of transport. Other species augment diffusion by using active ventilation, creating advective (bulk) flows that move air both within the tracheal system and in and out of the body [3]. Although active ventilation has been known and studied in insects since the 1800's, studies

*To whom all correspondence should be addressed: John S. Hochgraf, Tel: 1-603-969-4615, Email: jshochgraf@gmail.com.

†Abbreviations: RTC, Rhythmic tracheal compression.

Keywords: rhythmic tracheal compression, insect, beetle, respiration

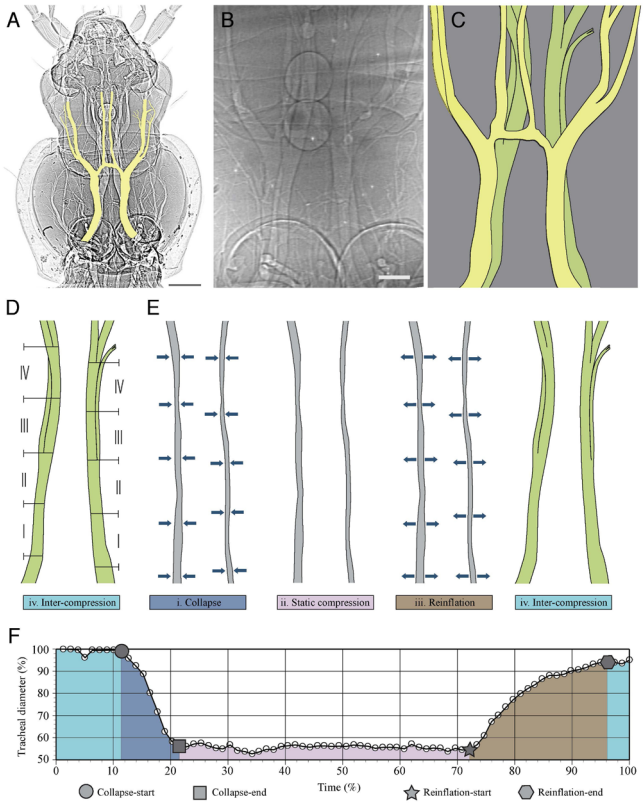

Figure 1. Rhythmic tracheal compression in the thoracic and head tracheae of *Platynus decentis*. (A) Synchrotron x-ray image of the thorax and head of *P. decentis*. The dorsal tracheal trunks are highlighted in yellow for emphasis. The posterior end of the two thoracic trunks connect directly to the large mesothoracic spiracles, located on the ventral side of the animal. The legs of the beetle were removed prior to imaging. For reference, the width of the prothorax is 2.9 mm. Scale bar, 0.5 mm. Image modified with permission of SPIE., from [27]. (B, C) The tracheal trunks analyzed in this study, shown in yellow (dorsal) and green (ventral). Scale bar, 200 µm. (D) The four regions analyzed for temporal progression of rhythmic tracheal compression (RTC), with IV oriented most anteriorly. (E) RTC comprises four distinct phases: (i) tracheal collapse, when the tubes are deformed to a smaller volume; (ii) static compression, during which the collapsed configuration of the tubes is maintained; (iii) reinflation of the tracheae to original volume; and (iv) inter-compression, the period between compression cycles. These phases are depicted in (F) relative to a full collapse and reinflation cycle, with collapse-start, collapse-end, reinflation-start, and reinflation end noted with symbols.

of diffusion have predominated, and the biomechanical mechanisms that underlie the production of advection are far less understood.

Rhythmic tracheal compression (RTC) is one mechanism for producing air flows in the system. Although tracheae are reinforced with thickenings in the wall called taenidia, as thin-walled tubes, they are capable of collapse. During RTC, portions of the tracheal system are cyclically compressed and reinflated, a process comprising four phases (Figure 1E, F): *collapse,* in which the tracheal tube experiences rapid (<1 s) decrease in volume; *static compression*, in which the tube is maintained compressed in a minimum volume state; *reinflation*, in which the tube expands rapidly to its initial resting volume in a time course similar to compression; and *inter-compression*, the resting period between subsequent compression cycles. This behavior was first brought to light by Westneat *et al*. [4], whose novel application of synchrotron phase-contrast x-ray imaging enabled the quantification of RTC in species of house cricket (*Achaeta domesticus*), carpenter ant (*Camponotus pennsylvanicus*), and carabid beetle (*Platynus decentis*), and who also identified the occurrence of compression in the orders Lepidoptera (butterflies and moths), Hemiptera (true bugs), Dermaptera (earwigs), Blattodea (cockroaches), and Odonata (dragonflies).

Since then, synchrotron imaging has been used to investigate the respiratory behaviors associated with RTC

in a small number of studies, revealing variation across taxa. The grasshopper *Schistocerca americana* employs tracheal and air sac compression during abdominal pumping [5], with the majority of the compression occurring in the abdomen, and only small portions observed in the thorax or head [6]. The carabid beetle *Pterostichus stygicus* exhibits synchronous tracheal compression in every body segment, including the legs (femur) and mouthparts (mandibles) [3]. Simultaneous recording of respiratory gases show that this beetle expels CO_2 with each compression cycle, demonstrating that RTC can augment gas exchange by advecting air in and out of the body. In a major thoracic trunk of the passalid beetle *Odontotaenius disjunctus*, some compressions exhibit directionality, with collapse directed posteriorly along the tube axis, and reinflation directed anteriorly [7]. RTC also occurs during development. Larvae of the tobacco hornworm *Manduca sexta* exhibit RTC, but the behavior was only observed under certain environmental conditions (specifically, with atmospheric P_{O2} less than 2 kPa), and only in larger specimens; larvae with body mass less than 0.2 g were not observed to compress their tracheae [8]. Pupae of the tenebrionid beetle *Zophobas morio* regularly employ RTC, but simultaneous recordings of hemolymph pressure and CO_2 demonstrate that tracheal compression only occurs when the spiracles are open [9]. In these pupae, the pressure created by the abdominal pump is great enough to deform the tracheal wall, displacing air and thereby creating advection. However, when all spiracles are closed and the tracheal system is sealed, the air is only compressed by ~2 percent, a negligible change in volume, which implies that x-ray observations of substantial tracheal compression could only occur when the insect has at least one spiracle open. Overall, the variance in behavior across groups suggests that RTC plays a diverse role in the respiratory physiology of insects.

Although components of RTC have been described in these species, we have very little knowledge of specific airflow patterns produced within the tracheal system. Mechanistically, airflow should depend on both the temporal and spatial patterns of RTC as well as the open/closed state of the spiracles. For example, tracheal collapse that propagates towards an open spiracle might function as a peristaltic pump and expel air from the tracheal tubes, whereas collapse that proceeds away from the spiracle could drive oxygen-rich air from the atmosphere deep into the tracheoles. Airflows within the main tracheal trunks of beetles have been characterized using estimates of volume displacement during compression, calculated from measurements of tracheal wall displacement. In the carabid beetle *Platynus decentis*, the estimated maximum airflow speed is on the order of 1 mm/s, with a Reynolds number much less than 1, which suggests that viscosity dominates and fluid inertia is negligible [10]. Such estimates have enabled recent theoretical and numerical studies of the effect of insect-inspired wall movements in single channels [11-13] and a network [14]. Intriguingly, these studies suggest that compressions that occur with a temporal phase lag can produce unidirectional flow, and that flows can be directed within a network. However, these theoretical studies did not use specific insect parameters for the modeling, simply because they were not available in the literature. A rigorous description of tracheal displacement patterns is needed to improve modeling for better understanding the fluid dynamics of gas transport within insect tracheal systems.

Here, we examine the kinematics of RTC in the main thoracic tracheal trunks in the carabid beetle *Platynus decentis* using live imaging with synchrotron x-rays. We address two questions related to the temporal and spatial patterns of tracheal compression. First, is tracheal compression directional? Specifically, we examine whether individual compressions along the length of a tube occur sequentially, which could lead to unidirectional or directed flow. Second, how stereotypic is RTC within and across individuals? Such patterns may lend insight into the biomechanical mechanisms that underlie its production.

MATERIAL AND METHODS

Animals

We examined the tracheal system in the thorax and head of *Platynus decentis*, a species that has been examined in one other study using similar methods [4]. Beetles were collected in ~15 cm pitfall traps in the woods at Argonne National Laboratory (Argonne, IL, USA). For up to 30 days prior to experiments, beetles were kept in a terrarium lined with soil and were provided with *ad libitum* water and food (dog chow). Both males and females were used but were not distinguished. A total of 11 individuals were imaged ($m = 50.5 \pm 5.4$ mg).

Synchrotron X-ray Imaging

We recorded live videos using synchrotron phase contrast x-ray imaging, using methods detailed in [15]. Data were collected at the Advanced Photon Source of Argonne National Laboratory at beamline XOR-32ID. Monochromatic x-rays (25 keV) were used, with images formed on a scintillator crystal (cerium-doped yttrium aluminum garnet) and recorded at 30 Hz using a video camera (Cohu 4920 or Cohu 2700, Cohu, San Diego, CA, USA). The distance between the insect and the scintillator was 70 cm. Two microscope lenses were used, either a 2X objective providing a field of view of 3.2 x 2.4 mm, or a 5X objective providing a field of view of 1.3 x 1.0 mm. Movies were downloaded to a Macintosh computer using

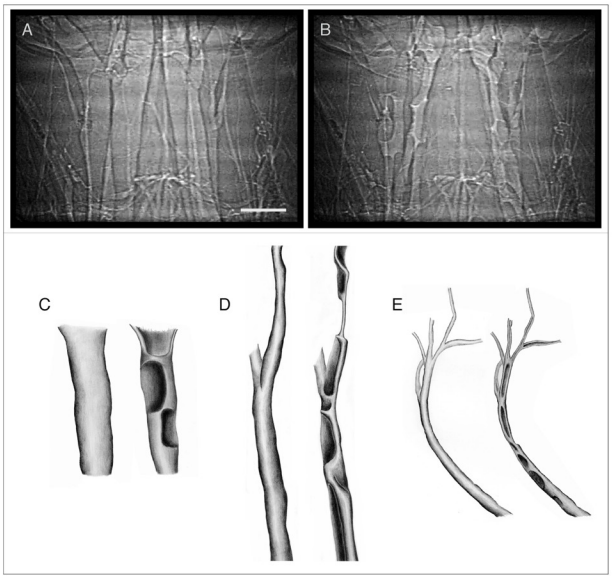

Figure 2. Deformation patterns in trachea appear as "dimples" in the tube wall. (A, B) Inflated and collapsed state of the dorsal and ventral tubes shown in Figure 1B, C. Scale bar, 200 μm. (C-E) Artist's interpretation of collapse patterns in dorsal (C) and ventral trunks, and smaller thoracic branch located near the lateral margin of the prothorax (E).

Final Cut Pro software (Apple, Cupertino, CA, USA).

In each trial, beetles were imaged individually in a custom container made of x-ray translucent polyimide film (Kapton, Dupont, DE, USA). The film was rolled into a cone and secured with scotch tape. With this design, the beetle could be mounted snugly in a head-down position, with the head oriented toward the small end of the cone. Cotton was placed at the posterior end of the beetle and secured with adhesive putty (Scotch adhesive putty, 3M, MN, USA), which served to keep the beetle in place. Despite this restraint, beetles had room to make small movements (including free dorsoventral movement of the abdomen). Both ends of the cone were open, allowing free access to ambient air. The cone was mounted on a translation stage, which allowed for fine positioning of the sample during imaging. Beetles were oriented with the ventral surface oriented orthogonally to the x-ray beam, providing a dorsoventral view (e.g., Figure 1A, B; Figure 2A, B). Because the x-ray images provide a projection view with all features in focus, all resolvable tracheae (~>10 μm) in the field of view were in focus.

Directional Axis of Compression

The direction of deformation of the tracheal wall during compression has been documented qualitatively as occurring either laterally or dorsoventrally [4], or it can be identified in published data where it was not explicitly identified [3,6-8,16]. We evaluated directionality of compression in the main dorsal and ventral thoracic tracheae, classifying the axis of deformation as "dorsoventral," "lateral," or "other." For compression that occurred in the dorsoventral axis, collapse was identified from darkening of the tracheae in the x-ray image, indicating volume displacement of air (as air is less dense than tissue). Usually these compressions appeared as rounded depressions forming "dimples" (Figure 2), and the adjacent length of tube maintained near-constant tracheal diameter throughout the compression cycle. (Note: "dimple" is commonly used in the engineering literature as a term for local inward depressions in the walls of cylinders, see for example [17-19]. We follow this convention.) In contrast, during lateral compression the tracheal walls were squeezed together in the lateral plane, manifesting as decreased tube diameter. Compressions categorized as "other" were those that were not obviously oriented in the lateral or dorsoventral directions. We tested the significance of the association between compression direction and specific tracheal tube (dorsal or ventral thoracic trunk) using Fisher's exact test.

Temporal Progression of Tracheal Compression

We analyzed the detailed temporal progression of compression in the main thoracic ventral tubes (Figure 1C-E) in five specimens (N = 5), with five compression cycles for each individual (n = 25). The ventral tracheal tubes were selected for analysis because they provided the clearest view due to their comparatively simple tube geometry and dearth of branching tubes. We quantified

progression of compression along the tube length by analyzing events in four approximately equal-sized zones (Figure 1D). We defined Region I as the tube segment anterior to the thoracic spiracles, and Region IV as posterior to the head. Regions II and III were spaced evenly between Regions I and IV. In the x-ray video, we visually identified the transitions between compression phases, referred to as events, for each region. We recorded the frame number for the occurrence of four events: collapse-start, collapse-end, reinflation-start, and reinflation-end (Figure 1D, E).

Collapse-start was identified by a rapid decrease in tracheal diameter, marking the transition between the resting inter-compression phase and dynamic compression phase of RTC. Collapse-end occurred at the transition between the decreasing diameter and constant diameter static-compression phases of RTC, when the diameter equilibrated around a constant minimum value. Similarly, reinflation-start marked the transition between the static compression and inflation phases, and was signified by an increase in tube diameter. Finally, reinflation-end completed the cycle and denoted the transition between the inflation and inter-compression phases.

In practice, we identified the duration of events by frame-by-frame analysis of the x-ray videos using ImageJ software [20]. By visual inspection of the tracheal tubes, the frame numbers corresponding to each event were recorded for each compression cycle in each trachea and region. Any frame that exhibited characteristics of a phase transition was included as part of the event. For example, a frame in which the tracheal diameter was observedly smaller than the previous frames was marked as tracheal collapse-start. Based on an uncertainty analysis (see Appendix A), the uncertainty associated with event identification was ±1.1 frames for collapse-start, ±1.6 frames for collapse-end, ±1.2 frames for inflation-start, and ±3.2 frames for inflation-end, corresponding to absolute durations of 0.04, 0.05, 0.04, and 0.11 s, respectively.

After events were identified, we ordered their temporal progression across the four regions from 1 to 4, using the start time of the event (*i.e.*, the first frame) for comparison. If the difference between start times of two events was less than the calculated uncertainty, they were considered to occur simultaneously. Assuming that actuation of the tube wall in each region occurred independently, we calculated the number of possible progression combinations as a permutation of four choosing four with replacement:

$$ {}^{n}P_{r} = n^{r} $$

$$ {}^{4}P_{4} = 4^{4} = 256 $$

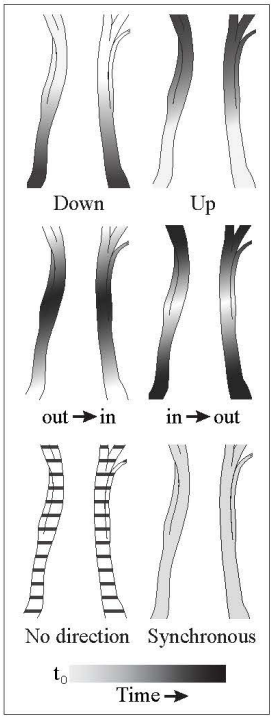

Figure 3. Possible temporal patterns of progression of collapse and reinflation in regions I-IV, depicted with shading from light to dark.

where n is the number of items that may be selected (n = 4 regions), and r is the number of items that are selected (r = 4 regions).

Although 256 permutations are available, a subset of these combinations are not physically possible. For example, the permutations [1, 1, 1, 3] and [1, 1, 1, 4] would represent that the first three regions actuated synchronously, followed by actuation of the fourth region. The true pattern can only be indicated as [1, 1, 1, 2], rendering the previous two iterations redundant. Using a custom Python script, we pruned the maximum 256 permutations to remove all such redundant combinations, leaving 75 combinations that represent all possible patterns of tube actuation (see Appendix A, Table S2). Of these, 22 were considered as not conducive to producing directional air flow (e.g., [1, 4, 2, 3]), and the fully synchronous combination would promote equal flow in both directions ([1 1 1 1]). The remaining 52 permutations comprise four types of directional behavior: up, down, in-out, and out-in (Figure 3). Although these terms correspond to anatomical orientations (here, "up"=anterior), we use this terminology as shorthand for convenience.

Pearson's χ^2 goodness of fit test was used to compare the frequency distribution of the experimentally observed RTC events with the expected number of observations for

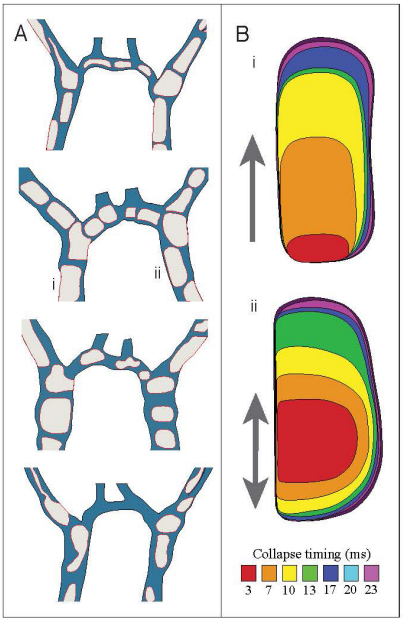

Figure 4. Variation of dimple patterns in the dorsal tracheae of *Platynus decentis*. (A) Locations where collapse occurred in four individual specimens, with dimples depicted in gray. (B) Dimple growth in one specimen, with (i) unilateral collapse occurring in one direction (anteriorly) along the central tube axis, and (ii) bilateral dimple growth occurring in both directions.

each directional behavior, assuming that the probability of each of the 75 different permutations was equal. Fisher's exact test was used to evaluate whether the collapse and inflation phases of RTC exhibited a significantly different number of unidirectional flow events.

Stereotypy of Dimpling

Throughout the tracheal-collapse phase of RTC, the dimples on the thoracic dorsal tracheal walls grew progressively larger until reaching a maximum size (Figure 4). To investigate the stereotypy of dimple formation, we used the polygon selection tool in ImageJ to measure the maximum area of a dimple once per cycle over the course of eight compression cycles, from which we calculated an area variance. We measured the area of two dimples per beetle in four beetles, for a total of eight different dimples. For comparison with measurement error, we also calculated the variance of eight repeated measurements of dimple area made on a single x-ray video frame (for each dimple). Levene's test for unequal variances was used to test for significant differences between these two measurements.

Statistics

Statistical analyses were conducted using JMP 9.0.0 software (2010 SAS Institute Inc) and Python (Python Software Foundation. Python Language Reference, version 3.7.0. Available at http://www.python.org). All tests were performed with a Type I error rate of α=0.05.

RESULTS

Kinematics of Tracheal Compression

The main thoracic dorsal and ventral tracheae exhibited different preferred directions of compression (Table 1; P<0.0001, Fisher's exact test). The dorsal tubes collapsed dorsoventrally (10 of 11 specimens), whereas the ventral tubes tended to collapse laterally (8 of 11). In two specimens, lateral compression was accompanied by apparent axial twisting of the ventral tubes.

Dorsoventral collapse was characterized by the formation of discrete, buckled regions in the tube wall, which gave the appearance of dimpling (Figures 2, 4). The specific location, size, and shape of dimples differed among individuals (Figure 4A). Within an individual, the location of dimple formation and direction of propagation was consistent from one compression cycle to the next.

Variation in the kinematics of dimple formation was observed within and among beetles. The majority of dimple formation can be characterized as one of two general types: bilateral or unilateral (Figure 4B). In bilateral formation, the dimple appeared to expand in the axial direction. Unilateral dimple growth also occurred along the tube axis, but in one primary direction. In either case, dimples spread outward until they reached the edge of the tracheal wall or a encountered another dimple. Some dimples exhibited highly irregular shapes. The variation in dimple area across compression cycles was not significantly different from the variation in the repeated measurement of a single dimple (Table 1). This result indicates that we could not distinguish a difference in area across compression cycles.

Timing and Directionality of Tracheal Compression

The average duration of each phase of tracheal compression within the four regions analyzed ranged from 0.22 to 0.26 s (Table 2). The average timing between the start of consecutive events across regions (e.g., the different between 1 to 2 and 2 to 3) was 0.03 ± 0.04 s (mean ± S.D.) for collapse and 0.05 ± 0.05 s for reinflation (N=200).

Along the length of the two ventral trunks, the regional temporal analysis revealed that 75 percent of collapse and reinflation events were synchronous, 17 percent showed a linear directionality, and the remainder showed some other pattern (See Appendix A, Figure S1). Table

Table 1. Variation of dimple size in *Platynus decentis*. The first and second rows display the standard deviations of dimple area for control samples (multiple measurements of dimple area on the same frame) and time-dependent samples (area measurements of the same dimple over the course of multiple compression cycles), respectively. Values are in units of μm². The third row contains the P-value associated with Levene's test for unequal variances.

Dimple #	1	2	3	4	5	6	7	8
Control SD	372	377	78	139	120	46	56	118
Sample SD	447	606	62	240	77	140	75	171
P-value	0.672	0.185	0.236	0.093	0.389	0.069	0.170	0.360

Table 2. Duration of compression events by region in *Platynus decentis.*

RTC phase	Region	N	Mean duration (s)	Standard deviation (s)
Collapse				
	I	50	0.26	0.08
	II	50	0.25	0.08
	III	50	0.25	0.08
	IV	50	0.22	0.09
Inflation				
	I	50	0.23	0.10
	II	50	0.24	0.10
	III	50	0.27	0.10
	IV	50	0.24	0.15

Table 3. Directionality of rhythmic tracheal compression in *Platynus decentis*. The frequency of the observed direction of tracheal collapse is compared to the expected number of event directions assuming each tube permutation theoretically capable of producing bulk flow has an equal probability of occurring.

RTC phase		Up	Down	Out-In	In-Out	Synchronous	No Direction	*N*
Collapse								
	Start	2	8	4	2	34	0	50
	End	0	9	4	0	37	0	50
Inflation								
	Start	6	1	7	0	35	1	50
	End	3	0	1	0	45	1	50
Expected								
	All	4.7	4.7	12.7	12.7	0.7	14.7	50

3 shows the number of observed frequencies for each of the six possible behaviors with respect to the four RTC events. The "Expected" row shows the predicted number of observations for each behavior if the 75 possible permutations were equally likely to occur. Table 4 shows the total number of observations vs. the predicted number of observations for each behavior if the 75 possible permutations were equally likely to occur. A comparison of these permutation frequencies vs. the observed patterns shows that the frequency distributions of the experimental and expected observations are fundamentally different (Pearson's χ^2 goodness of fit, $P<0.0001$). Table 5 shows the observed frequency distributions of unidirectional flow behavior in the inflation and collapse phases of RTC. Fisher's exact test suggests that the frequency distribution of observed unidirectional events is significantly different

Table 4. Directionality of rhythmic tracheal compression in *Platynus decentis*. Combined observations from each tracheal event (the marginal distribution of each event in Table 3) and the expected number of observations assuming each of the 75 tube permutations has equal probability of occurring.

RTC Phase	Up	Down	Out-In	In-Out	Synchronous	No Direction	*N*
Observed	11	18	16	2	151	2	200
Expected	18.7	18.7	50.7	50.7	2.7	58.7	200

Table 5. Directionality of rhythmic tracheal compression in *Platynus decentis*. The direction of actuation start and end are combined to show aggregate counts by RTC phase.

RTC Phase	Up	Down	Other	*N*
Collapse	2	17	81	100
Inflation	9	1	90	100

(Fisher's exact test, $P<0.0001$).

DISCUSSION

We examined spatial and temporal patterns of rhythmic tracheal compression in the main thoracic trunks of the carabid beetle *Platynus decentis*. The majority of the observed events did not show directionality of propagation of collapse—along the length of the two ventral trunks, most collapse and reinflation events were synchronous, far greater than expected, and only a small percentage showed a linear directionality. This overall lack of directionality contrasts with the bidirectional compression pattern found in the superior cephalic trachea of the passalid beetle *Odontotaenius disjunctus* [7]. Its bidirectional compression consists of a collapse that propagates posteriorly toward the thoracic spiracle at a rate of 4.4 ± 1.4 mm/s and a reinflation that occurs anteriorly almost twice as fast as collapse, at a rate of 9.6 ± 1.3 mm/s. This difference between species may reflect variation in compression mechanisms or tracheal morphology, or it may result from differences in body size—*P. decentis* is more than two orders of magnitude smaller in mass (~50 mg vs. ~1.6 g). Detailed analyses of tracheal compression patterns have been conducted on only a small number of taxa, yet there are an immense number of beetle species and insects (estimated recently between 0.9 to 2.1 million and 5.4 to 7.2 million, respectively; [21]). Thus, it remains unclear how representative these patterns are across the diversity of insects, and what role body size plays in RTC.

Alternatively, it is possible that appreciable directionality does occur during RTC in the ventral thoracic trunks of *Platynus decentis*, but it occurs at a faster time scale than could be resolved with our measurements. Given the calculated uncertainty of event identification, this would mean that any hypothetical propagation of collapse would occur in less than ~50 ms, and propagation of reinflation would occur in less than ~110 ms. In fact, our finding that local deformations of the tracheal wall develop as rounded dimples that propagate outward means that at some scale, directional compression dynamics must exist.

However, the mechanical effect on the air within the tubes during and across such compression cycles is not known. Recent theoretical studies by Aboelkassem and Staples have begun to probe simplified flow systems inspired by RTC to develop new microfluidic pumping strategies and to understand the mechanical implications of this behavior. Using both analytical and numerical approaches, the majority of this work has considered the dynamics of flow created by multiple wall deformations characterized by equal displacement, but with a phase lag between deformations. In these models, the channel length is much greater than its width, the Reynolds number is low ($Re<<1$), and the wall displacement does not completely occlude the channel, with displacements up to 70 percent of the channel width. When the phase lag between displacement locations is 0° or 180°, no net flow occurs, but other values produce positive flows, with maximum flows occurring at ~60-70° in two-dimensional models [11,12,22] and 105° in a three-dimensional model [13]. A follow-up to these single-channel models is a branching model that incorporates network geometry similar to and inspired by the thoracic tracheal system of *P. decentis* [14]. Results from this model demonstrate that different combinations of actuation and phasing can produce directed flow through specific channels.

Although these theoretical studies provide valuable insight into the fluidic behaviors that might possibly result from RTC, they did not use insect-specific parameters in regard to compression dynamics, simply because they were not available at the time. Future modeling studies that incorporate specific tracheal kinematics (such as

those from *P. decentis* reported here) are needed to understand the effect of variation in compression behavior on airflow mechanics. Another important consideration to incorporate in future models is the effect of physiologically relevant boundary conditions. Specifically, the upstream and downstream pressures in the tracheae surrounding locations of compression should, in theory, strongly influence flow behavior. The determinants of these pressures include the geometry of the tracheal system and the metabolic demand for O_2 and output of CO_2 at the tissues, and state of the spiracles (either open, closed, or fluttering). In the passalid beetle *Odontotaenius disjunctus*, for example, one chance observation of a mesothoracic spiracle showed that tracheae nearby compressed only when the spiracle was closed [7]. To displace air, at least one other spiracle in the animal must have been open [9]. In this scenario, the compression near the closed spiracle must have pushed air deeper into the tracheal system, away from the spiracle. In contrast, a previous study of RTC in the carabid beetle *Pterostichus stygicus* that measured gas exchange patterns showed that compressions were correlated with peaks in CO_2 emission, showing that compressions pushed air across the spiracles and out of the body. Together, these studies suggest that insects employ multiple strategies for transporting air in the tracheal system during RTC.

The variation of compression across and within individual tracheae in this study also provides insight into the biomechanical mechanism that produces RTC. The main dorsal tracheae exhibited a proclivity to collapse dorsoventrally, whereas the main ventral tracheae collapsed laterally. The dimpling pattern of deformation varied both along the length of a trachea and across individuals, but it did not vary across compression cycles within an individual. Tracheae are not muscularized [23], so the physical mechanisms that produce collapse can only include deformation due to mechanical impingement of the tube by some other aspect of anatomy (for example, movement of an apodeme), or by a fluidic pressure difference across the tracheal wall. This pressure difference could arise from an increase in pressure in the surrounding hemolymph, a decrease in pressure in the air within the trachea, or some combination of both. The specific location of dimple formation may result from local differences in tracheal properties, which may include variations in tracheal diameter or wall thickness, taenidial patterns, or material properties of the tracheal tissue. Recent studies of such tracheal properties are revealing inhomogeneities that might be important for compression mechanics [24-26]. For example, taenidia in the American cockroach *Periplaneta americana* were observed to branch or fuse along the circumference of the tubes, which might represent sites for local stress concentrations where collapse is initiated. New studies that integrate such biomechanical considerations with complementary physiological measurements will help to reveal the multiple roles of rhythmic tracheal compression in insects.

Acknowledgments: We thank Mark Westneat, Jon Harrison, Wah-Keat Lee, and Kamel Fezzaa for assistance with x-ray data collection and for many helpful discussions of tracheal compression in insects over the years. This study was supported by the National Science Foundation under grants 0938047 and 1558052 to J.J.S. and by the Virginia Tech Institute for Critical Technology and Applied Science (ICTAS). This research used resources of the Advanced Photon Source, a U.S. Department of Energy (DOE) Office of Science User Facility operated for the DOE Office of Science by Argonne National Laboratory under Contract No. DE-AC02-06CH11357.

REFERENCES

1. Harrison JF. Tracheal system. Encyclopedia of Insects. 2nd ed. Elsevier; 2009. pp. 1011–5.
2. Harrison JF. Respiratory system. Encyclopedia of Insects. 2nd ed. Elsevier; 2009. pp. 889–95.
3. Socha JJ, Lee WK, Harrison JF, Waters JS, Fezzaa K, Westneat MW. Correlated patterns of tracheal compression and convective gas exchange in a carabid beetle. J Exp Biol. 2008;211(21):3409–20.
4. Westneat MW, Betz O, Blob RW, Fezzaa K, Cooper WJ, Lee WK. Tracheal respiration in insects visualized with synchrotron X-ray imaging. Science. 2003;299(5606):558–60.
5. Greenlee KJ, Henry JR, Kirkton SD, Westneat MW, Fezzaa K, Lee WK, et al. Synchrotron imaging of the grasshopper tracheal system: morphological and physiological components of tracheal hypermetry. Am J Physiol Regul Integr Comp Physiol. 2009;297(5):R1343–50.
6. Harrison JF, Waters JS, Cease AJ, VandenBrooks JM, Callier V, Klok CJ, et al. How locusts breathe. Physiology (Bethesda). 2013;28(1):18–27.
7. Waters JS, Lee WK, Westneat MW, Socha JJ. Dynamics of tracheal compression in the horned passalus beetle. Am J Physiol Regul Integr Comp Physiol. 2013;304(8):R621–7.
8. Greenlee KJ, Socha JJ, Eubanks HB, Pedersen P, Lee WK, Kirkton SD. Hypoxia-induced compression in the tracheal system of the tobacco hornworm caterpillar, *Manduca sexta*. J Exp Biol. 2013;216(12):2293–301.
9. Pendar H, Kenny MC, Socha JJ. Tracheal compression in pupae of the beetle *Zophobas morio*. Biol Lett. 2015;11(6):20150259.
10. Westneat MW, Socha JJ, Lee WK. Advances in biological structure, function, and physiology using synchrotron x-ray imaging. Annu Rev Physiol. 2008;70:119–42.
11. Aboelkassem Y, Staples AE. Flow transport in a microchannel induced by moving wall contractions: a novel micropumping mechanism. Acta Mech. 2012;223(3):463–80.
12. Aboelkassem Y, Staples AE. A bioinspired pumping model for flow in a microtube with rhythmic wall contractions. J Fluids Structures. 2013;42:187–204.
13. Aboelkassem Y, Staples AE. A three-dimensional model for flow pumping in a microchannel inspired by insect respira-

tion. Acta Mech. 2014;225(2):493–507.
14. Aboelkassem Y, Staples AE. Selective pumping in a network: insect-style microscale flow transport. Bioinspir Biomim. 2013;8(2):026004.
15. Socha JJ, Westneat MW, Harrison JF, Waters JS, Lee WK. Real-time phase-contrast x-ray imaging: a new technique for the study of animal form and function. BMC Biol. 2007;5:6.
16. Lee WK, Socha JJ. Direct visualization of hemolymph flow in the heart of a grasshopper (*Schistocerca americana*). BMC Physiol. 2009;9(1).
17. Horák J, Lord GJ, Peletier MA. Cylinder buckling: the mountain pass as an organizing center. SIAM J Appl Math. 2006;66(5):1793–824.
18. Kobayashi T, Mihara Y, Fujii F. Path-tracing analysis for post-buckling process of elastic cylindrical shells under axial compression. Thin Walled Struct. 2012;61:180–7.
19. Sun M, Hyer MW. Use of material tailoring to improve buckling capacity of elliptical composite cylinders. AIAA J. 2008;46(3):770–82.
20. Schneider CA, Rasband WS, Eliceiri KW. NIH Image to ImageJ: 25 years of image analysis. Nat Methods. 2012;9(7):671–5.
21. Stork NE, McBroom J, Gely C, Hamilton AJ. New approaches narrow global species estimates for beetles, insects, and terrestrial arthropods. Proc Natl Acad Sci USA. 2015;112(24):7519–23.
22. Aboelkassem Y, Staples AE. Stokeslets-meshfree computations and theory for flow in a collapsible microchannel. Theor Comput Fluid Dyn. 2013;27(5):681–700.
23. Whitten JM. Comparative anatomy of the tracheal system. Annu Rev Entomol. 1972;17:373–402.
24. Webster MR, De Vita R, Twigg JN, Socha JJ. Mechanical properties of tracheal tubes in the American cockroach (*Periplaneta americana*). Smart Mater Struct. 2011;20(9):094017.
25. Becker WR, Webster MR, Socha JJ, De Vita R. Variation in the mechanical properties of tracheal tubes in the American cockroach. Smart Mater Struct. 2014;23(5):057001.
26. Webster MR, Socha JJ, Teresi L, Nardinocchi P, De Vita R. Structure of tracheae and the functional implications for collapse in the American cockroach. Bioinspir Biomim. 2015;10(6):066011.
27. Socha JJ, De Carlo F. Use of synchrotron tomography to image naturalistic anatomy in insects. Developments in X-Ray Tomography VI. San Diego (CA): SPIE; 2008. 70780A–70787.

Appendix A.

Contents:

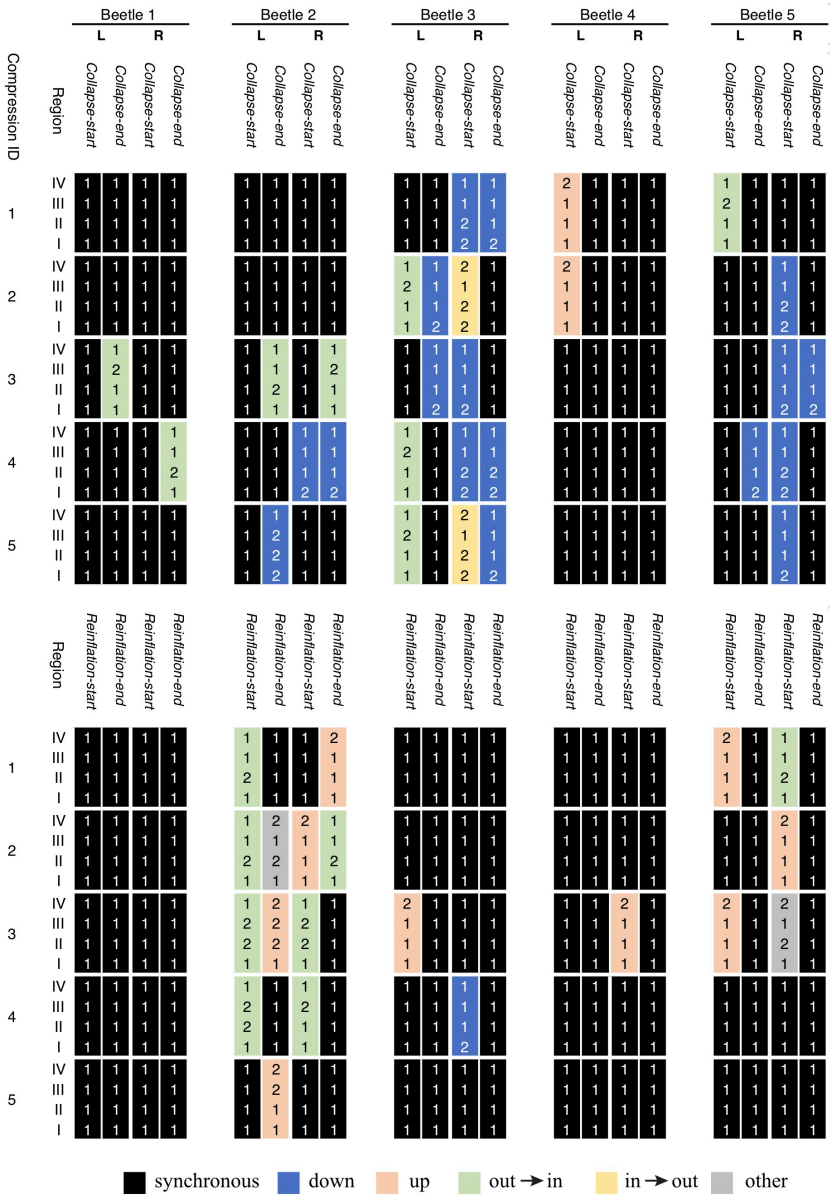
Beetle 1
Beetle 2
Beetle 3
Beetle 4
Beetle 5
L
R
Compression ID
Region
Collapse-start
Collapse-end
Reinflation-start
Reinflation-end
IV
III
II
I
synchronous
down
up
out → in
in → out
other

Figure S1. Summary of temporal progression of collapse and reinflation events in the ventral tracheae of five specimens of *Platynus decentis*. The numbers refer to temporal order of events, progressing from 1 to 4. Collapse is shown in the top row, and reinflation in the bottom row, sorted in 5 columnar groups by individual. The left and right trunks are indicated. Each compression is color-coded to show occurrence of synchronous, down, up, out-in, in-out, and other patterns of temporal progression.

Table S1: Summary permutations of tracheal progression order by region.

Direction	*N*	%
Down	7	9.3%
In-Out	19	25.3%
No Direction	22	29.3%
Out-In	19	25.3%
Synchronous	1	1.3%
Up	7	9.3%
Total	75	100.0%

Table S2: Theoretical permutations of tracheal progression order by region.

ID	Tube Region				Classification
	I	II	III	IV	
1	1	1	1	1	Synchronous
2	1	1	1	2	Up
3	1	1	2	1	Out-In
4	1	1	2	2	Up
5	1	1	2	3	Up
6	1	1	3	2	Out-In
7	1	2	1	1	Out-In
8	1	2	1	2	Other
9	1	2	1	3	Other
10	1	2	2	1	Out-In
11	1	2	2	2	Up
12	1	2	2	3	Up
13	1	2	3	1	Out-In
14	1	2	3	2	Out-In
15	1	2	3	3	Up
16	1	2	3	4	Up
17	1	2	4	3	Out-In
18	1	3	1	2	Other

19	1	3	2	1	Out-In
20	1	3	2	2	Out-In
21	1	3	2	3	Other
22	1	3	2	4	Other
23	1	3	3	2	Out-In
24	1	3	4	2	Out-In
25	1	4	2	3	Other
26	1	4	3	2	Out-In
27	2	1	1	1	Down
28	2	1	1	2	In-Out
29	2	1	1	3	In-Out
30	2	1	2	1	Other
31	2	1	2	2	In-Out
32	2	1	2	3	In-Out
33	2	1	3	1	Other
34	2	1	3	2	Other
35	2	1	3	3	In-Out
36	2	1	3	4	In-Out

Appendix A: Theoretical permutations of tube actuation. (CONT)

ID	Tube Region				Classification
	I	II	III	IV	
37	2	1	4	3	Other
38	2	2	1	1	Down
39	2	2	1	2	In-Out
40	2	2	1	3	In-Out
41	2	2	2	1	Down
42	2	2	3	1	Out-In
43	2	3	1	1	Out-In
44	2	3	1	2	Other
45	2	3	1	3	Other
46	2	3	1	4	Other
47	2	3	2	1	Out-In
48	2	3	3	1	Out-In
49	2	3	4	1	Out-In
50	2	4	1	3	Other
51	2	4	3	1	Out-In
52	3	1	1	2	In-Out
53	3	1	2	1	Other
54	3	1	2	2	In-Out
55	3	1	2	3	In-Out

56	3	1	2	4	In-Out
57	3	1	3	2	Other
58	3	1	4	2	Other
59	3	2	1	1	Down
60	3	2	1	2	In-Out
61	3	2	1	3	In-Out
62	3	2	1	4	In-Out
63	3	2	2	1	Down
64	3	2	3	1	Other
65	3	2	4	1	Other
66	3	3	1	2	In-Out
67	3	3	2	1	Down
68	3	4	1	2	Other
69	3	4	2	1	Out-In
70	4	1	2	3	In-Out
71	4	1	3	2	Other
72	4	2	1	3	In-Out
73	4	2	3	1	Other
74	4	3	1	2	In-Out
75	4	3	2	1	Down

Determination of Uncertainty in Visual Identification of Events

Synchrotron x-ray phase contrast imaging has provided researchers and scientists with a window through which to view the *in vivo* mechanics of insect respiration [1]. Although synchrotron phase contrast imaging enables many internal structures to be visualized, as with any imaging technique, the resulting images are far from perfect. Tracheal structures in insects are highly amenable to visualizing because of the large contrast between the density of air and the density of tissue, but the boundary of the tracheal wall can sometimes be difficult to discern due to noise in the image and image blur from the moving wall during a dynamic tracheal compression cycle. Changes in effective tissue density along with the frequent pixilation of physiological boundaries impose limitations on the efficacy of tracking of the tracheal wall during tracheal compression. Manual digitization provides a quantitative estimate of the location of the wall, but it is time-consuming. We chose to identify phases of tracheal compression by frame-by-frame visual analysis in ImageJ [2]. Here, we compare these methods by applying both manual digitization and visual identification to ten compression cycles and quantifying the uncertainty.

Manual Digitization

Figure S1: Manual digitization of a tracheal tube using ImageJ and the Point Picker plugin. The trachea runs horizontally, and the two wall edges can be seen as dark lines.

Data Acquisition

Synchrotron x-ray video files were imported into ImageJ, and contrast and levels were adjusted to enhance the visibility of the tracheal tube walls [1]. The ‘Point Picker’ plugin was

used to place points on the images. Two points about 25 pixels apart were selected on the upper edge of the tracheal tube. A length of roughly 25 pixels was chosen because it allowed the digitized portion of tube wall to remain relatively straight regardless of broader curvature of the tracheal tube. Eight points were chosen at even intervals between the two initial points, yielding

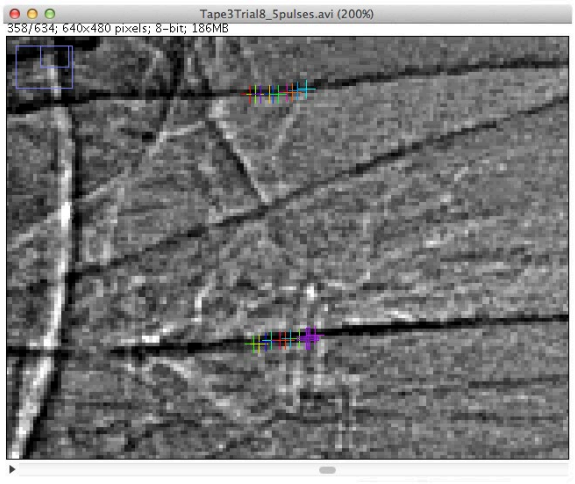

a total of ten data points along the top edge of the tube.

Two points were placed on the lower edge of the tube directly opposite the boundary points on the top edge so that they reflected orthogonally across the tube diameter. Eight points were spaced evenly between the two boundary points along the lower edge for a grand total of twenty data points. Figure S1 is a screenshot from ImageJ showing a typical example of point placement.

The x,y coordinates of the points were imported into Matlab, and linear regression was used to fit curves to the top and bottom boundaries of the tube. A perpendicular bisector was superimposed on the bottom boundary, and the distance between the intersection with the top

and bottom tube edges was defined as the tracheal tube diameter. The process was repeated for each frame of the tracheal compression cycle.

Data Processing

A smoothing spline was fit to a plot of tracheal tube diameter versus frame number. Numerical differentiation was used to solve for the zero slope point to find the transition between rhythmic tracheal compression phases. The zero slope point of the derivative of tube diameter occurs when the diameter has stopped changing, providing means to identify the transitions between RTC phases: collapse-start, collapse-end, reinflation-start, and reinflation-end. If the zero slope point occurred between two frames, the greater frame number was selected as the true frame of the event. The frame number calculated using this technique was considered to be the true frame of incidence for a specified event.

Visual Event Extraction

Data Acquisition

Video sequences were imported into ImageJ and visually scanned for transitions between RTC phases. The researchers' best estimate of the frame denoting each event (collapse-start, collapse-end, reinflation-start, and reinflation-stop) was recorded.

Uncertainty Analysis

The drawback associated with visual data extraction is that accuracy depends on the ability of the researcher to discern visually finite differences in tube movement and position, which may vary between individual researchers.

Two sources of error were considered when calculating the total uncertainty ascribed to the events marking the transitions between RTC phases. The first source of error derives from the visual extraction of events. The events in five compression cycles from two image sequences of perceptively different quality were visually extracted. The process was repeated three times with a minimum of twelve hours between sessions over the course of several days. The data for the two image sequences were pooled to determine the standard error of repeated visual measurements.

The two image sequences were manually digitized using the protocol described above. The results of the manual digitization were considered as a benchmark to which the visual extraction results were compared. The uncertainty between the two techniques was calculated, accounting for error associated with visually identifying the true frame number of an event. The total uncertainty for each event was calculated to be the Euclidean norm of the two constituent uncertainties taken at 95% confidence. For collapse-start, collapse-stop, reinflation-start and reinflation-stop, the respective uncertainties were calculated to be +/- 1.1 frames, +/- 1.6 frames, +/- 1.2 frames and +/- 3.2 frames, corresponding to absolute durations of 0.04, 0.05, 0.04, and 0.11 s, respectively.

References

1. Socha JJ, Westneat MW, Harrison JF, Waters JS, Lee WK. Real-time phase-contrast x-ray imaging: a new technique for the study of animal form and function. BMC Biology. 2007;5:6.
2. Schneider CA, Rasband WS, Eliceiri KW. NIH Image to ImageJ: 25 years of image analysis. Nature Methods. 2012;9(7):671-5.